

Communication

Acceleration of the Computation of the Method of Moments EFIE Impedance Matrix From an Updated Fraunhofer Criterion

Christophe Bourlier^{ib}

Abstract—This communication deals with the acceleration of the computation of the impedance matrix obtained from the electric field integral equation (EFIE) discretized by the Galerkin method of moments (MoM) with Rao–Wilton–Glisson basis functions. The elements of the impedance matrix need to calculate a double integral (quadruple integral) over two planar triangles, which is typically done from two numerical Gauss–Legendre integrations. For far-field interactions, this integration can be done analytically by introducing a criterion for which the resulting closed-form expression is valid. This approximation is tested on a sphere and a concave cavity-shaped object, for which the results show that the time saving factor is about 20, with a mean difference of 0.1–0.5 dB on the radar cross section (RCS) compared to that obtained from two numerical integrations.

Index Terms—Electric field integral equation (EFIE), fast algorithm, method of moments (MoM), radar cross section (RCS).

I. INTRODUCTION

The method of moments (MoM) [1] has been commonly used to solve electromagnetic scattering problems. It transforms integral equations into a matrix equation. For small problems, the resulting linear system can be solved from the lower-upper (LU) decomposition. For larger problems, iterative solvers like the conjugate gradient and their improved versions [2], [3] can be employed, in which accelerations are accounted for [4], [5]. Another family of fast iterative solvers has also been developed. The problem geometry is subdivided into subdomains (blocks) and the problem solution is then reduced in order to successively solve a set of impedance submatrix equations [6], [7], in which accelerations are included [8], [9].

Whatever the solver, some elements of the impedance matrix must be calculated. This step requires the evaluation of a double integration (quadruple 1-D integral) over the source and observation facets (of triangular shapes in our case, since the Rao–Wilton–Glisson basis functions are used to discretize the electric field integral equation (EFIE) from the Galerkin MoM). Usually, two Gauss–Legendre integrations with n_{Gauss} points are applied, both on the source and observation triangles. For large n_{Gauss} , this step can be time consuming. The purpose of this communication is to accelerate this stage when the observation facet is in the far-field with regard to the source facet. Then, a criterion is derived by updating the conventional Fraunhofer criterion to our problem. When this criterion is valid, it is shown that the two integrations can be done analytically, which reduces the computing time. In addition, it is important to underline that the closed-form expression is only valid for planar facets and that the complexity of assembling the matrix is not changed.

Manuscript received December 20, 2019; revised June 23, 2020; accepted August 30, 2020. Date of publication September 29, 2020; date of current version May 5, 2021.

The author is with the IETR Laboratory, Institut d’Electronique et des Technologies numéRique, UMR CNRS 6164, University of Nantes, 44035 Nantes, France (e-mail: christophe.bourlier@univ-nantes.fr).

Color versions of one or more of the figures in this communication are available online at <https://ieeexplore.ieee.org>.

Digital Object Identifier 10.1109/TAP.2020.3025440

0018-926X © 2020 IEEE. Personal use is permitted, but republication/redistribution requires IEEE permission.

See <https://www.ieee.org/publications/rights/index.html> for more information.

The communication is organized as follows. Section II presents the MoM, whereas Section III derives the criterion and gives the closed-form expression of an element of the impedance matrix. Section IV presents numerical results, and Section V gives concluding remarks.

II. METHOD OF MOMENTS

In this communication, to compute the field scattered by a perfectly conducting object, the EFIE is solved from the MoM. In addition, the Galerkin method is applied with the Rao–Wilton–Glisson basis functions. This leads to solving the linear system $\bar{\mathbf{Z}}\mathbf{X} = \mathbf{b}$, where $\bar{\mathbf{Z}}$ is the impedance matrix, \mathbf{b} a vector related to the incident wave, and \mathbf{X} is the unknown vector. The time convention $e^{-j\omega t}$ is used throughout this communication.

The element $Z_{m,n}$ of the impedance matrix $\bar{\mathbf{Z}}$, corresponding to the interaction between two edges m (observation) and n (source) of a facet couple (p, q) is expressed as [2]

$$Z_{m,n} = \frac{c_{m,n}}{A_p A_q} \iint_{T_p} \iint_{T_q} \left[\frac{1}{4} \boldsymbol{\rho}_m^p \cdot \boldsymbol{\rho}_n^q - \frac{1}{k^2} \right] \frac{e^{-jkD_{p,q}}}{D_{p,q}} d\mathbf{R}_p d\mathbf{R}_q \quad (1)$$

where $c_{m,n} = L_m L_n s_{m,n} / (4\pi)$, in which $\{L_{m,n}\}$ are the edge lengths and $s_{m,n} = \pm 1$, $\{A_{p,q}\}$ are the triangle areas, $\boldsymbol{\rho}_{m,n}^{p,q} = \mathbf{V}_{m,n}^{p,q} - \mathbf{R}_{p,q}$, in which $\mathbf{V}_{m,n}^{p,q}$ is the position vector of the vertex unshared by the edge (m, n) and belonging to the facet (p, q) . In addition, $D_{p,q} = \|\mathbf{R}_p - \mathbf{R}_q\|$ and k is the wavenumber which equals $2\pi/\lambda$, where λ is the wavelength.

Assuming a plane incident wave, a component b_n of the vector \mathbf{b} associated with the source edge n and facet q is [2]

$$b_n = -\frac{j}{\omega\mu} \frac{L_n s_n}{2A_q} \iint_{T_q} \boldsymbol{\rho}_n^q \cdot \hat{\mathbf{p}}_{\text{inc}} e^{-\mathbf{k}_{\text{inc}} \cdot \mathbf{R}_q} d\mathbf{R}_q \quad (2)$$

where ω is the wave pulsation and μ is the permeability of the surrounding medium. In addition, $\hat{\mathbf{p}}_{\text{inc}}$ (either vertical, $\hat{\mathbf{v}}_{\text{inc}}(\theta)$, or horizontal, $\hat{\mathbf{h}}_{\text{inc}}(\phi)$) and \mathbf{k}_{inc} are the polarization and incident wave vectors, respectively, both defined in spherical coordinates from the angles $(\theta_{\text{inc}}, \phi_{\text{inc}})$. Solving the linear system $\mathbf{X} = \bar{\mathbf{Z}}^{-1}\mathbf{b}$, the components $\{a_n\}$ of the vector \mathbf{X} are found. The scattered far-field is then expressed as

$$\mathbf{E}_{\text{sca}}^\infty(\mathbf{R}_0) = -\frac{j\omega\mu e^{-jkR_0}}{8\pi R_0} \sum_{p=1}^{P_{\text{Facet}}} \sum_{m=1}^{M_{\text{Edge}}} \frac{L_m a_m s_m}{A_p} \times \iint_{T_p} \boldsymbol{\rho}_m^p e^{j\mathbf{k}_{\text{sca}} \cdot \mathbf{R}_p} d\mathbf{R}_p \quad (3)$$

where P_{Facet} is the number of facets and M_{Edge} the number of edges associated with the facet p . In addition, R_0 is the distance from the receiver to the phase origin of the object. The scattering coefficient is then expressed as

$$\text{SC}_{p_{\text{inc}} p_{\text{sca}}} = \lim_{R_0 \rightarrow \infty} 2\sqrt{\pi} R_0 \frac{\mathbf{E}_{\text{sca}}^\infty \cdot \hat{\mathbf{p}}_{\text{sca}}}{\mathbf{E}_{\text{inc}}^\infty \cdot \hat{\mathbf{p}}_{\text{inc}}} \quad (4)$$

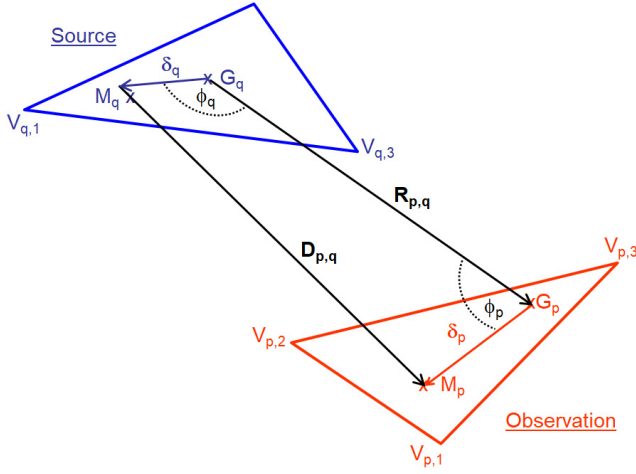


Fig. 1. Interaction of a facet source q with an observation facet p . The point $G_{p,q}$ is the gravity center of the triangle (p, q) and the point $M_{p,q}$ is the integration point which spans the triangle (p, q) .

where $p_{\text{inc}} = \{\theta, \phi\}$ and $p_{\text{sca}} = \{\theta, \phi\}$. The subscripts “inc” and “sca” stand for incident and scattered (waves), respectively. The receiver polarization basis $(\hat{\mathbf{k}}_{\text{sca}}, \hat{\mathbf{v}}_{\text{sca}}, \hat{\mathbf{h}}_{\text{sca}})$ can be defined in a similar way as that of the incident field $(\hat{\mathbf{k}}_{\text{inc}}, \hat{\mathbf{v}}_{\text{inc}}, \hat{\mathbf{h}}_{\text{inc}})$, in which θ_{sca} and ϕ_{sca} are the receiver (scattering) angles. The radar cross section $\text{RCS}_{p_{\text{inc}}p_{\text{sca}}}$ is obtained by taking the squared modulus of $\text{SC}_{p_{\text{inc}}p_{\text{sca}}}$.

Equation (1) shows that $Z_{m,n}$ requires the calculation of two numerical integrations over the surfaces of the triangles T_p and T_q . This is done from two-fold Gauss–Legendre integrations. In this communication, we propose to derive them from a closed-form expression. The singularity, which occurs for $D_{p,q} = 0$, is computed from the work published by Sheng et al. [10].

III. APPROXIMATION OF $Z_{m,n}$

As shown in Fig. 1, the distance $D_{p,q} = \|\mathbf{D}_{p,q}\| = \|\overrightarrow{M_q M_p}\|$, where $\overrightarrow{M_q M_p} = \overrightarrow{M_q G_q} + \overrightarrow{G_q G_p} + \overrightarrow{G_p M_p} = \mathbf{R}_{p,q} + \delta$, where $\mathbf{R}_{p,q} = \overrightarrow{G_q G_p}$ and $\delta = \overrightarrow{M_q G_q} + \overrightarrow{G_p M_p} = \delta_p - \delta_q$. If $\|\overrightarrow{G_q G_p}\| = R_{p,q} \gg \|\delta\| = \delta$, the distance D can be expanded over $R_{p,q}$ up to the second order as

$$D_{p,q} = \sqrt{R_{p,q}^2 + \delta^2 + 2R_{p,q}\delta \cos \phi} \approx R_{p,q} + \delta \cos(\phi) + \frac{\sin^2(\phi)\delta^2}{2R_{p,q}} \quad (5)$$

where $\phi = (\widehat{\mathbf{R}_{p,q}}, \delta)$. The term in δ is related to the local behavior of a plane wave, whereas δ^2 is related to the local behavior of a spherical wave. The Fraunhofer criterion is obtained from (5) by neglecting the term in δ^2 . In Green’s function, this approximation is satisfied if $\delta^2 \sin^2 \phi / (2R_{p,q})$ does not exceed λ/n_0 (typically n_0 is an integer ranging from 10 to 20). This leads for $kD_{p,q}$, to

$$\frac{\delta^2 \sin^2 \phi}{2 R_{p,q}} \leq \frac{\lambda}{n_0}. \quad (6)$$

The maximum value of δ , named Δ , equals

$$\begin{aligned} \Delta &= \max \|\delta_p - \delta_q\| = \max \|\delta_p\| + \max \|\delta_q\| \\ &\approx \sum_{i=\{p,q\}} \max[(x_{M_i} - x_{G_i})^2 + (y_{M_i} - y_{G_i})^2 \\ &\quad + (z_{M_i} - z_{G_i})^2]^{1/2}. \end{aligned} \quad (7)$$

If the criterion (7) is satisfied, then

$$D \approx R_{p,q} + \delta \cos(\phi) = R_{p,q} + \frac{\mathbf{R}_{p,q}}{R_{p,q}} \cdot (\delta_p - \delta_q). \quad (8)$$

In (1), the double integral can be simplified as

$$\begin{aligned} I_{m,n} &= \frac{1}{A_p A_q} \iint_{T_p} \iint_{T_q} \left[\frac{1}{4} \rho_m^p \cdot \rho_n^q - \frac{1}{k^2} \right] \frac{e^{-jkD_{p,q}}}{D_{p,q}} d\mathbf{R}_p d\mathbf{R}_q \\ &\approx \frac{e^{-jkR_{p,q}}}{A_p A_q R_{p,q}} \iint_{T_p} \iint_{T_q} \left[\frac{1}{4} \rho_m^p \cdot \rho_n^q - \frac{1}{k^2} \right] \\ &\quad \times e^{-jk\hat{\mathbf{R}}_{p,q} \cdot \delta_p} e^{+jk\hat{\mathbf{R}}_{p,q} \cdot \delta_q} d\mathbf{R}_p d\mathbf{R}_q \end{aligned} \quad (9)$$

where $\hat{\mathbf{R}}_{p,q} = \mathbf{R}_{p,q}/R_{p,q}$. Using the variable transformation $\delta_p = \overrightarrow{G_p M_p} = \overrightarrow{G_p O} + \overrightarrow{OM_p} = \overrightarrow{OM_p} - \overrightarrow{OG_p} = \overrightarrow{OM_p} - \mathbf{R}_{G_p} \Rightarrow \overrightarrow{OM_p} = \mathbf{R}_p = \delta_p + \mathbf{R}_{G_p}$, where the point O stands for the phase origin, the above integral can be simplified as

$$I_{m,n} = \frac{e^{-jkR_{p,q}}}{R_{p,q}} \left[\frac{1}{4} \mathbf{J}_{q,m} \cdot \mathbf{J}_{p,n}^* - \frac{1}{k^2} K_q K_p^* \right] \quad (10)$$

where

$$K_i = \frac{1}{A_i} \iint_{T'_i} e^{jk\hat{\mathbf{R}}_{p,q} \cdot \delta_i} d\delta_i \quad (11)$$

and

$$\begin{aligned} \mathbf{J}_{i,m} &= \frac{1}{A_i} \iint_{T'_i} (\mathbf{V}_m^i - \mathbf{R}_{G_i} - \delta_i) e^{jk\hat{\mathbf{R}}_{p,q} \cdot \delta_i} d\delta_i \\ &= (\mathbf{V}_m^i - \mathbf{R}_{G_i}) K_i - \mathbf{L}_i \end{aligned} \quad (12)$$

where

$$\mathbf{L}_i = \frac{1}{A_i} \iint_{T'_i} \delta_i e^{jk\hat{\mathbf{R}}_{p,q} \cdot \delta_i} d\delta_i. \quad (13)$$

It is important to underline that the integration domain T'_i of the facet $i = (p, q)$ is now defined from the gravity center \mathbf{R}_{G_i} . In addition, the integrals K_i (scalar) and \mathbf{L}_i (vector) do not depend on the edge and only depend on the distance $R_{p,q}$ and on the triangle i defined from its three vertices. Owing to the presence of the term \mathbf{V}_m^i , the integral $\mathbf{J}_{i,m}$ depends on the edge m . As shown in Appendix, the integrals K_i and \mathbf{L}_i can be derived analytically. In conclusion, an element of the impedance matrix can be computed analytically from (10) if

$$\frac{\Delta^2 \sin^2 \phi}{2 R_{p,q}} \approx \frac{\Delta^2}{2R_{p,q}} \leq \frac{\lambda}{n_0}. \quad (14)$$

In practice, the angle ϕ cannot be determined numerically since it depends on the integration variables. Then, $\phi = \pi/2$ is chosen as an upper limit of the criterion. For two given triangles p and q , the coordinates of their gravity centers $\{\mathbf{R}_{G_p}, \mathbf{R}_{G_q}\}$ are known and then the distance $R_{p,q} = \|\mathbf{R}_{G_p} - \mathbf{R}_{G_q}\|$ is computed. Moreover, Δ is computed from (7). Typically, $\Delta = a_p + a_q$, where a_i is the circle radius circumscribed to the triangle i ($i = \{p, q\}$).

It is important to underline that integrals (2) and (3) can also be computed analytically, since

$$\frac{1}{A_p} \iint_{T_i} \rho_m^i e^{s \cdot \mathbf{R}_i} d\mathbf{R}_i = \mathbf{V}_m^i K_i - \mathbf{L}_i. \quad (15)$$

For (2), $s = -\mathbf{k}_{\text{inc}}$ and for (3), $s = \mathbf{k}_{\text{sca}}$. In addition, the variable transformation over δ_i is not applied (the three vertices of the triangle i are defined from the phase origin O).

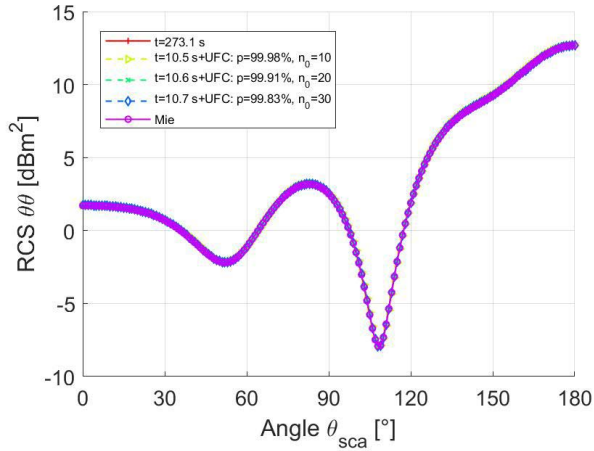


Fig. 2. Bistatic RCS in dBm^2 versus the scattering angle θ_{sca} . $\theta_{\text{inc}} = 0$, $\phi_{\text{inc}} = 0$ and $\phi_{\text{sca}} = 0$. The illuminated object is a sphere of radius $a = 0.6\lambda_0$.

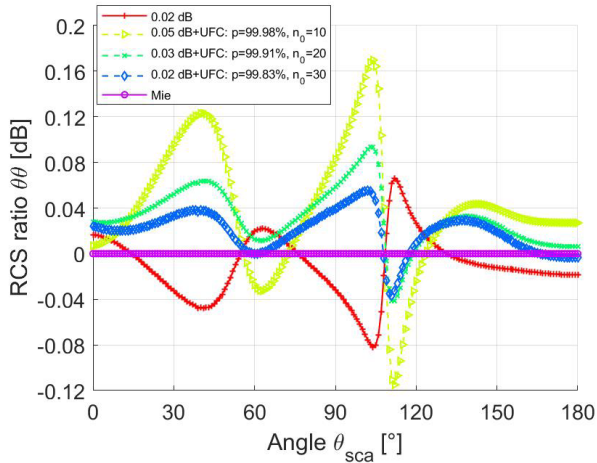


Fig. 3. Ratio $\text{RCS}/\text{RCS}|_{\text{Mie}}$ in decibel scale versus the scattering angle θ_{sca} . The parameters are the same as in Fig. 2.

IV. NUMERICAL RESULTS

The wavelength in free space λ is 1 m and the polarization is $\theta\theta$.

First, to test the accuracy of the proposed method, a sphere is considered, for which the field scattered by a plane wave is known exactly from the Mie series [11].

Fig. 2 plots the bistatic RCS in dBm^2 versus the scattering angle θ_{sca} . The incidence angles are $\theta_{\text{inc}} = 0$, $\phi_{\text{inc}} = 0$ and $\phi_{\text{sca}} = 0$ is the scattering azimuthal angle. To better highlight the differences, Fig. 3 plots the corresponding ratio $\text{RCS}/\text{RCS}|_{\text{Mie}}$ in decibel scale (becomes a difference) versus the scattering angle θ_{sca} , where $\text{RCS}|_{\text{Mie}}$ is the reference Mie solution. The sphere has a radius $a = 0.6\lambda_0$ and the number of edges is $N_{\text{Edge}} = 6279$, corresponding to an edge mean length of $0.05\lambda_0$. As shown in Figs. 2 and 3, this value ensures a very good agreement between the results obtained from two Gauss–Legendre integrations, for which the number of points is $n_{\text{Gauss}} = 6$.

In Fig. 3, in the legend, the first number gives the mean value of $10|\log_{10}(\text{RCS}/\text{RCS}|_{\text{Mie}})|$ over $\theta_{\text{sca}} \in [0; \pi]$. The acronym ‘‘UFC’’ means updated Fraunhofer criterion. The second number p gives the percentage of facet pairs which are in far-field and for which the approximation is applied. The integer n_0 is the number of points per wavelength, corresponding to a phase error of λ_0/n_0 to estimate

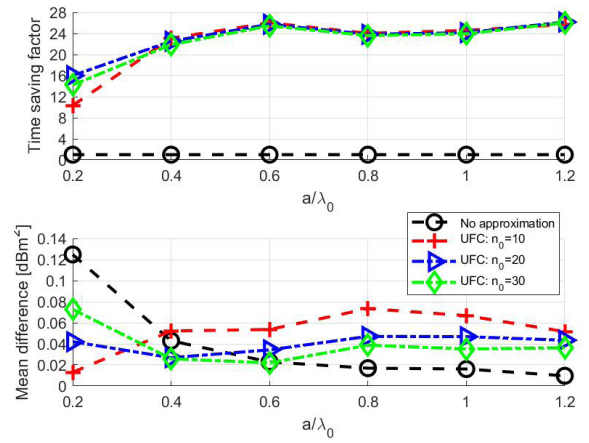


Fig. 4. Top: Time saving factor versus a/λ_0 . Bottom: Mean difference on the RCS ratio versus a/λ_0 .

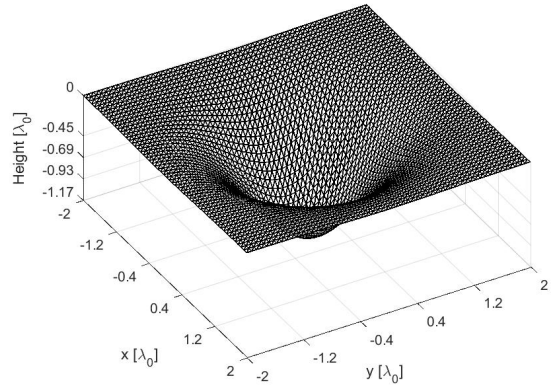


Fig. 5. Example of a concave cavity-shaped object with $L_x = L_y = 4\lambda_0$. The number of edges is $N_{\text{Edge}} = 9633$ and the edge mean length is $0.08\lambda_0$.

Green’s function. As expected, as n_0 increases, the results better match with those of Mie and are very similar to those computed from two numerical integrations.

In Fig. 2, in the legend, the first number t gives the computing time to calculate the impedance matrix. In comparison to two numerical integrations, the time saving factor is of the order of 25. As n_0 decreases, the number of the facet pairs p in far-field increases and then, all the elements of the impedance matrix are computed from the approximation. The time saving factor is approximately proportional to $\eta_t = n_{\text{Gauss}}^2/C_{\text{App}}$, where n_{Gauss}^2 is the complexity of two numerical integrations and C_{App} , that of the approximation. Theoretically, this value is equal to one, but it differs from one in practice because the calculation of the analytical expression needs some multiplications. This explains why in Fig. 2, η_t is smaller than $n_{\text{Gauss}}^2 = 6^2 = 36$. Fig. 2 also shows that η_t is little sensitive to n_0 .

Fig. 4 plots the time saving factor η_t versus a/λ_0 (N_{Edge} ranging from 669 to 24321) and at the bottom, the mean ratio $10|\log_{10}(\text{RCS}/\text{RCS}|_{\text{Mie}})|$ over $\theta \in [0; \pi]$ is plotted versus a/λ_0 . As the radius a increases, the gain in time saving is nearly constant, equal to approximately 25, and the mean difference does not exceed 0.08 dB. The percentage of facet pairs in far-field over $a/\lambda_0 \in [0.2, 1.2]$ ranges from $\{0.9836, 0.9919, 0.9978\}$ to $\{0.9995, 0.9998, 0.9999\}$ for $n_0 = \{30, 20, 10\}$, respectively.

To produce strong interactions between the facets, a concave cavity-shaped object is considered to produce multiple reflections. The geometry is shown in Fig. 5. It is defined as

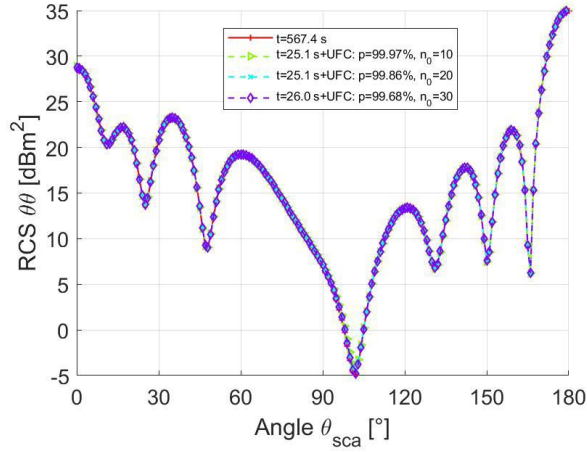


Fig. 6. RCS in dBm^2 versus the scattering angle θ_{sca} . $\theta_{\text{inc}} = 0$, $\phi_{\text{inc}} = 0$ and $\phi_{\text{sca}} = 0$. A concave cavity-shaped object is considered (Fig. 5).

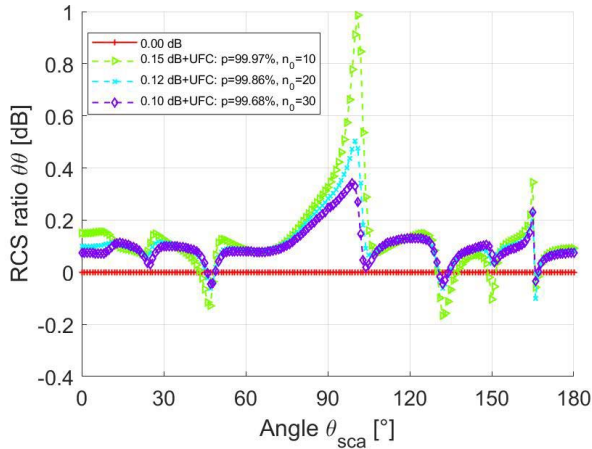


Fig. 7. Ratio RCS/RCS_0 in decibel scale versus the scattering angle θ_{sca} . The parameters are the same as in Fig. 6.

$z(x, y) = -A \exp(-x^2/a_1^2 - y^2/b_1^2)$ where $a_1 = L_x/4$, $b_1 = L_y/4$, $A = a_1 e^{1/2}/\sqrt{2}$ and L_x and L_y are the lengths of the object (defined for $z = 0$ corresponding to the top of Fig. 5) with respect to the x - and y -directions, respectively. In addition, the number A is chosen such that the absolute values of the maximum slopes with respect to the x - and y -directions are equal to one in order to produce a dihedral effect (at least two reflections).

Fig. 6 plots the RCS in dBm^2 versus the scattering angle θ_{sca} . $\theta_{\text{inc}} = 0$, $\phi_{\text{inc}} = 0$ and $\phi_{\text{sca}} = 0$. Fig. 7 plots the ratio RCS/RCS_0 in decibel scale versus the scattering angle θ_{sca} . The parameters are the same as in Fig. 6 and the number RCS_0 is the RCS calculated without approximation.

Fig. 6 shows a very good agreement between the RCS computed without approximation and those obtained from the approximation. Like for the sphere, the time saving factor is of the order of 21. In Fig. 7, the difference decreases as n_0 increases, and it increases when the RCS level in Fig. 6 takes low values. For these particular values, a better precision is required.

Fig. 8 plots the time saving factor versus L_x/λ_0 ($L_y = L_x$ and N_{Edge} ranging from 5208 to 29800). At the bottom, the RCS ratio between the proposed method and that without approximation is plotted in decibel scale (becomes a difference) versus L_x/λ_0 . As we can see, the gain in time saving is little sensitive to the length L_x

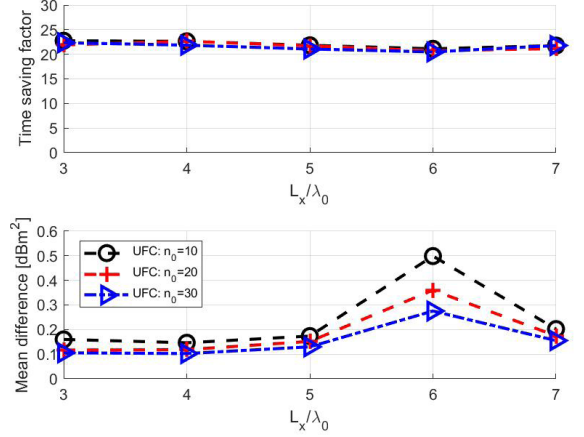


Fig. 8. Top: Time saving factor versus L_x/λ_0 ($L_y = L_x$). Bottom: Mean difference on the RCS ratio versus a/λ_0 .

and the mean difference does not exceed 0.5 dB. As n_0 increases, this value slightly decreases.

V. CONCLUSION

In this communication, from the derivation of a far-field criterion, the elements of the EFIE impedance matrix are computed from a closed-form expression. This approximation avoids to calculate these elements from two numerical integrations, which can be time consuming. The numerical results showed that the proposed method offers a time saving factor of the order of 25 for $n_{\text{Gauss}} = 6$, whereas for $n_{\text{Gauss}} = 3$ it equals 6 (not shown in the communication). This number is directly related to n_{Gauss}^2 , which corresponds to the complexity of the two numerical integrations. The choice of n_{Gauss} depends on the expected accuracy (related to the surface curvature, calculation in near or far-field, ...). In addition, for the $\phi\phi$ polarization, results (not depicted here) show that the approximation gives better results in comparison to the $\theta\theta$ polarization.

APPENDIX

DERIVATION OF THE INTEGRAL FOR A TRIANGULAR SHAPE

This appendix presents the derivation of the double integral (9). In simplex coordinates, any 2-D integral on a triangular domain T can be converted as ([2, eq. (9.29)])

$$\iint_T f(\mathbf{R}) d\mathbf{R} = 2A \int_0^1 \int_0^{1-\alpha} f(\alpha, \beta) d\alpha d\beta \quad (\text{A1})$$

where $\mathbf{R} = (1 - \alpha - \beta)\mathbf{V}_1 + \alpha\mathbf{V}_2 + \beta\mathbf{V}_3$ and $(\mathbf{V}_1, \mathbf{V}_2, \mathbf{V}_3)$ are the coordinates of the three vertices of the triangle T of area A . Then

$$K(\mathbf{s}) = \frac{1}{A} \iint_T e^{j\mathbf{s} \cdot \mathbf{R}} d\mathbf{R} = 2e^{j\mathbf{s} \cdot \mathbf{V}_1} \times \int_0^1 \int_0^{1-\alpha} e^{j\mathbf{s} \cdot (\mathbf{V}_2 - \mathbf{V}_1)\alpha} e^{j\mathbf{s} \cdot (\mathbf{V}_3 - \mathbf{V}_1)\beta} d\alpha d\beta \quad (\text{A2})$$

where \mathbf{s} is a constant vector (independent of \mathbf{R}). After some tedious but straightforward algebra, we obtain ([2, eq. (9.44)])

$$K(\mathbf{s}) = \frac{2Ae^{j\mathbf{s} \cdot \mathbf{V}_1}}{s_3 - s_2} \left(\frac{1 - e^{j\mathbf{s} \cdot \mathbf{V}_3}}{s_3} - \frac{1 - e^{j\mathbf{s} \cdot \mathbf{V}_2}}{s_2} \right) \quad (\text{A3})$$

where $s_1 = s \cdot \mathbf{V}_1$, $s_2 = s \cdot (\mathbf{V}_2 - \mathbf{V}_1)$ and $s_3 = s \cdot (\mathbf{V}_3 - \mathbf{V}_1)$. In addition, since $e^{js} \approx 1 + js$ for $|s| \ll 1$, we can show that

$$K(s) = 2e^{js_1} \begin{cases} (1 + js_2 - e^{js_2})/s_2^2, & \text{if } s_3 = 0 \\ (1 + js_3 - e^{js_3})/s_3^2, & \text{if } s_2 = 0 \\ e^{js_3}[(1 - js_3) - 1]/s_3^2, & \text{if } s_2 = s_3 \\ 1/2, & \text{if } s_2 = s_3 = 0. \end{cases} \quad (\text{A4})$$

The above equation is useful to avoid numerical problems. Applying the same way for $L(s)$, we show that

$$\begin{aligned} L(s) &= \iint_{\mathbf{T}} \mathbf{R} e^{j\mathbf{s} \cdot \mathbf{R}} d\mathbf{R} = 2Ae^{js_1} \int_0^1 \int_0^{1-\alpha} d\alpha d\beta \\ &\quad \times [(1 - \alpha - \beta)\mathbf{V}_1 + \alpha\mathbf{V}_2 + \beta\mathbf{V}_3] e^{js_2\alpha} e^{js_3\beta} \\ &= \mathbf{V}_1 F_0(s) - j(\mathbf{V}_2 - \mathbf{V}_1) \frac{\partial K}{\partial s_2} - j(\mathbf{V}_3 - \mathbf{V}_1) \frac{\partial K}{\partial s_3}. \end{aligned} \quad (\text{A5})$$

From (A3), the partial derivatives are expressed as

$$\begin{cases} \frac{\partial K}{\partial s_2} = \frac{2Ae^{js_1}}{s_3 - s_2} \left[\frac{K(s)}{2Ae^{js_1}} + \frac{1 + e^{js_2}(js_2 - 1)}{s_2^2} \right] \\ \frac{\partial K}{\partial s_3} = \frac{\partial K}{\partial s_2} \Big|_{(s_2, s_3) \rightarrow (s_3, s_2)}. \end{cases} \quad (\text{A6})$$

In addition,

$$\frac{\partial K}{\partial s_2} = 2e^{js_1} \begin{cases} [-2 - js_2 + e^{js_2}(2 - js_2)]/s_2^3, & \text{if } s_3 = 0 \\ [2 + 2js_3 - s_3^2 - 2e^{js_3}]/s_3^2, & \text{if } s_2 = 0 \\ [2 + e^{js_3}(s_3^2 + 2js_3 - 2)]/(2s_3^3), & \text{if } s_2 = s_3 \\ j/6, & \text{if } s_2 = s_3 = 0. \end{cases} \quad (\text{A7})$$

In conclusion, K_i expressed from (11) is obtained from (A3) by setting $s = k\hat{\mathbf{R}}_{p,q}$, for which the triangle i is defined from its three vertices. In addition, L_i [see (13)] is obtained from (A5) by setting

$s = k\hat{\mathbf{R}}_{p,q}$ and $\delta_i = \mathbf{R}$, for which the three vertices of the facet i are defined from their gravity center \mathbf{R}_{G_i} .

REFERENCES

- [1] R. F. Harrington, *Field Computation by Moment Method*. New York, NY, USA: Macmillan, 1968.
- [2] W. C. Gibson, *The Method of Moments in Electromagnetics*, Eds. London, U.K.: CRC, 2008.
- [3] A. Quarteroni, R. Sacco, and F. Saverio, *Méthodes Numériques: Algorithmes, Analyse et Applications*. New York, NY, USA: Springer-Verlag, 2007.
- [4] R. Coifman, V. Rokhlin, and S. Wandzura, "The fast multipole method for the wave equation: A pedestrian prescription," *IEEE Antennas Propag. Mag.*, vol. 35, no. 3, pp. 7–12, Jun. 1993.
- [5] C.-C. Lu and W. C. Chew, "Fast far-field approximation for calculating the RCS of large objects," *Microw. Opt. Technol. Lett.*, vol. 8, no. 5, pp. 238–241, 1995.
- [6] V. V. S. Prakash and R. Mittra, "Characteristic basis function method: A new technique for efficient solution of method of moments matrix equations," *Microw. Opt. Technol. Lett.*, vol. 36, no. 2, pp. 95–100, Jan. 2003.
- [7] C. Bourlier, S. Bellez, H. Li, and G. Kubickie, "Sub-domain decomposition iterative method combined with ACA: An efficient technique for the scattering from a large highly conducting rough sea surface," *IEEE Trans. Antennas Propag.*, vol. 63, no. 2, pp. 659–666, Feb. 2015.
- [8] K. Zhao, M. N. Vouvakis, and J.-F. Lee, "The adaptive cross approximation algorithm for accelerated method of moments computations of EMC problems," *IEEE Trans. Electromagn. Compat.*, vol. 47, no. 4, pp. 763–773, Nov. 2005.
- [9] C. Li and R. Mittra, "Characteristic basis function method for fast analysis of 3-D scattering from objects buried under rough surfaces," *IEEE Trans. Geosci. Remote Sens.*, vol. 57, no. 8, pp. 5252–5265, Aug. 2019.
- [10] W. T. Sheng, Z. Y. Zhu, K. Yang, and M. S. Tong, "Efficient evaluation of weakly singular integrals arising from electromagnetic surface integral equations," *IEEE Trans. Antennas Propag.*, vol. 61, no. 6, pp. 3377–3381, Jun. 2013.
- [11] L. Tsang, J. A. Kong, and K.-H. Ding, *Scattering of Electromagnetic Waves, Theories and Applications*, Ed. Hoboken, NJ, USA: Wiley, 2000.